Materials Transactions, JIM, Vol. 36, No. 3 (1995), pp. 391 to 398

Preparation of Bulky Amorphous Zr-Al-Co-Ni-Cu Alloys by Copper Mold Casting and Their Thermal and Mechanical Properties

Akihisa Inoue, Tao Zhang and Tsuyoshi Masumoto

Institute for Materials Research, Tohoku University, Sendai 980-77, Japan

Bulky amorphous alloys were found to form in Zr-Al-M (M=Co, Ni, Cu) systems by arc melting on a copper hearth. The largest thickness for glass formation is 6.1 mm for $Zr_{60}Al_{10}Co_3Ni_9Cu_{18}$, 6.8 mm for $Zr_{60}Al_{15}Co_5Ni_{15}Cu_5$ and 6.2 mm for $Zr_{55}Al_{20}Co_{17.5}Ni_{2.5}Cu_5$. The optimum composition for glass-forming ability shifts from the Cu-rich side to the Co-rich side through the Ni-rich side with increasing Al content from 10 to 20%. The use of a metallic mold casting process enabled the formation of amorphous cylinders with the largest diameter of 7 mm for the three alloys. The compositional effect for the large glass-forming ability has also been discussed by taking the present data into consideration. The cast amorphous $Zr_{60}Al_{10}Co_3Ni_9Cu_{18}$ alloy subjected to tensile testing exhibits distinct serrated flow before final fracture. The generation of the serrated flow is noticed because the alloy has a ductile nature which enables the momentary stop of the shear sliding. The Young's modulus, tensile fracture strength and fracture elongation are 97 GPa, 1510 MPa and 2.0%, respectively. The fracture occurs along the maximum shear plane and the fracture surface consists of a well-developed vein pattern. The size of their veins is about 10 times as large as that for the melt-spun ribbon and hence the shear deformation region occurs in a much wider region for the cast alloy, indicating the necessity of a larger amount of energy up to final fracture. The finding of the amorphous alloys with the large glass-forming ability and the extremely ductile nature is important for the subsequent development of metallic glassy materials.

(Received August 26, 1994)

Keywords: *bulk amorphous alloy, metallic mold casting, glass-forming ability, critical cooling rate, supercooled liquid, glass transition, high mechanical strength*

I. Introduction

Recently, we have found that amorphous alloys with large glass-forming ability form in a number of alloy systems such as Mg-Ln-TM[1][2], Ln-Al-TM[3][4], Zr-Al-TM[5]-[7] and Ti-Zr-TM[7]-[9] etc. (Ln=lanthanide metal, TM=transition metal). It has subsequently been reported that the large glass-forming ability enables the preparation of bulky amorphous alloys by using various preparation techniques of metallic mold casting[10][11], high-pressure die casting[12]-[14] and water quenching[15]-[17]. The maximum sample thickness for the formation of an amorphous phase reaches about 7 mm for Mg-Cu-Y system, 10 mm for La-Al-Ni-Cu system and 16 mm for Zr-Al-Ni-Cu system. The largest sample thickness for the Zr-Al-Ni-Cu amorphous alloys is obtained by quenching the molten alloy in a quartz tube into water.

Little is known about the preparation of bulk amorphous alloys in Zr-Al-TM system by the metallic mold casting method, presumably because of the difficulty of casting into copper molds resulting from high viscosity of the molten alloys. Furthermore, no data on the mechanical properties including tensile strength have been obtained for the bulky Zr-Al-TM alloys, though their properties have been reported[8]-[10] for bulky Mg-Ln-TM and Ln-Al-TM amorphous alloys in which the formation by metallic mold casting and high-pressure die casting is easier because of their lower melting temperatures and lower viscosities. It is very important to investigate the possibility of preparing bulky amorphous Zr-Al-TM alloys by the metallic mold casting method and to examine the tensile strength, deformation mode and fracture behavior of the bulky alloys, because of the expectation that the Zr-based alloys exhibit the highest strength, the best corrosion resistance and the lowest coefficient of thermal expansion among the Mg-, Ln- and Zr-based alloy systems.

This paper aims to present the composition range in which bulky amorphous alloys in Zr-Al-Co-Ni-Cu penternary system form by the metallic mold casting method, the compositional dependence of the maximum sample thickness for formation of the amorphous phase and the mechanical properties, deformation mode and fracture behavior of the bulky amorphous alloys.

II. Experimental Procedure

Ternary, quaternary and penternary alloys with alloy compositions of $Zr_{60}Al_{10}M_{30}$, $Zr_{60}Al_{15}M_{25}$ and $Zr_{55}Al_{20}M_{25}$ (M=Co, Ni and Cu) were prepared by arc melting mixtures of pure Zr, Al and M metals in an argon atmosphere. The alloys in the range of 10 to 20%Al were chosen because they had the widest supercooled liquid region before crystallization and the largest glass-forming ability[5][6][16]. The arc-melted ingots were used for the determination of a critical sample thickness for formation of an amorphous phase. The determination was made through the examination of a cross sectional structure in the central region by optical microscopy (OM) and X-ray diffractometry. The OM observation was made after etching for 60 s with a 10% hydrofluoric acid-

distilled water solution at 298 K. For the alloys with large critical thicknesses for formation of an amorphous phase, bulky cylindrical samples with a constant length of 50 mm and different diameters were prepared by injection casting of the melt into copper molds. The injection pressure was fixed to be 0.15 MPa. For comparison, an amorphous ribbon with a cross section of about 0.02×8 mm^2 was also produced by the single roller melt spinning method in an argon atmosphere. The amorphicity of the as-cast samples was examined by X-ray diffractometry, optical microscopy and differential scanning calorimetry (DSC). Yield and fracture strength values in tensile and compressive applied loads were measured at strain rates of 5.5×10^{-4} and 1.1×10^{-3} respectively, by using an Instron-type tensile testing machine. The shapes and dimensions for the specimens are a cylinder with a gauge diameter of 2.0 mm and a gauge length of 10 mm for the tensile specimen and a cylinder with a diameter of 2.5 mm and a height of 5.0 mm for the compressive specimen. The tensile and compressive specimens were prepared by mechanical polishing the cast cylinders with a diameter of 7 mm. The deformation mode, fracture behavior and fracture surface appearance were examined by scanning electron microscopy.

III. Results

1. Compositional dependence of glass-forming ability

Figures 1 to 3 show the compositional dependence of the maximum sample thickness for formation of an amorphous phase for arc-melted $Zr_{60}Al_{10}(Co, Ni, Cu)_{30}$, $Zr_{60}Al_{15}(Co, Ni, Cu)_{25}$ and $Zr_{55}Al_{20}(Co, Ni, Cu)_{25}$ alloys, respectively. It is seen that the large glass-forming ability with the critical sample thickness above 5.0 mm is obtained in the composition range of 0 to 5%Co, 5 to 12%Ni and 15 to 22%Cu for the $Zr_{60}Al_{10}M_{30}$ alloys, 0 to 7%Co, 8 to 23%Ni and 2 to 13%Cu for the $Zr_{60}Al_{15}M_{25}$ alloys, and 0 to 7%Co, 14 to 24%Ni and 0 to 14%Cu for the $Zr_{55}Al_{20}M_{25}$ alloys. Furthermore, the largest thickness for formation of the amorphous phase in each alloy system is 6.1 mm for $Zr_{60}Al_{10}Co_3Ni_9Cu_{18}$, 6.8 mm for $Zr_{60}Al_{15}Co_5Ni_{15}Cu_5$ and 6.2 mm for $Zr_{55}Al_{20}Co_{17.5}Ni_{2.5}Cu_5$, indicating that the glass-forming

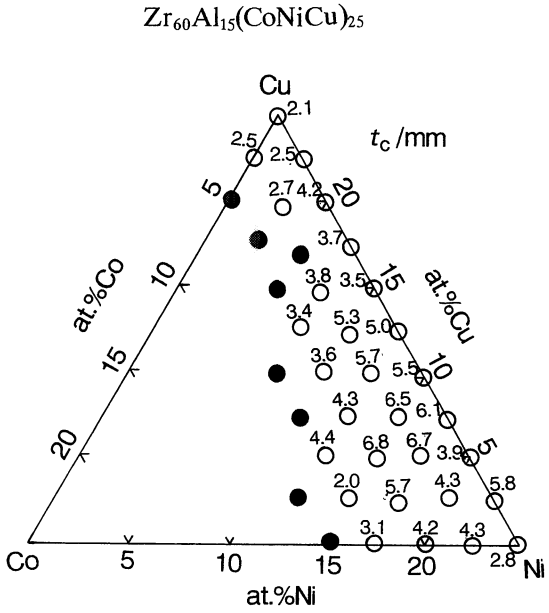

Fig. 2 Compositional dependence of the maximum sample thickness (t_c) for formation of an amorphous phase in $Zr_{60}Al_{15}(Co, Ni, Cu)_{25}$ alloys prepared by arc melting.

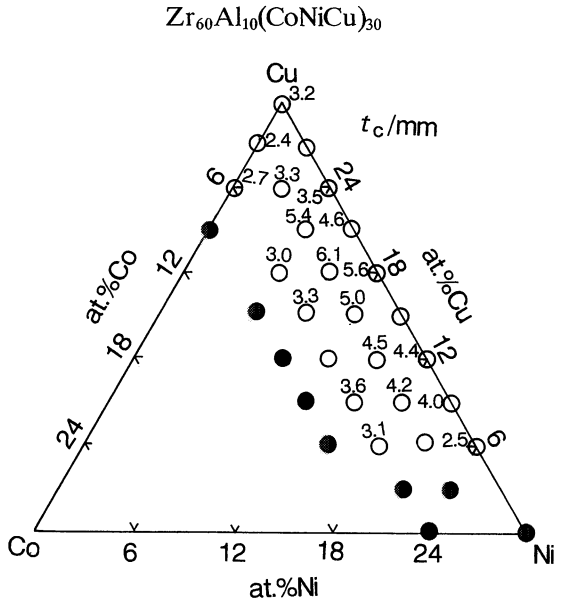

Fig. 1 Compositional dependence of the maximum sample thickness (t_c) for formation of an amorphous phase in $Zr_{60}Al_{10}(Co, Ni, Cu)_{30}$ alloys prepared by arc melting.

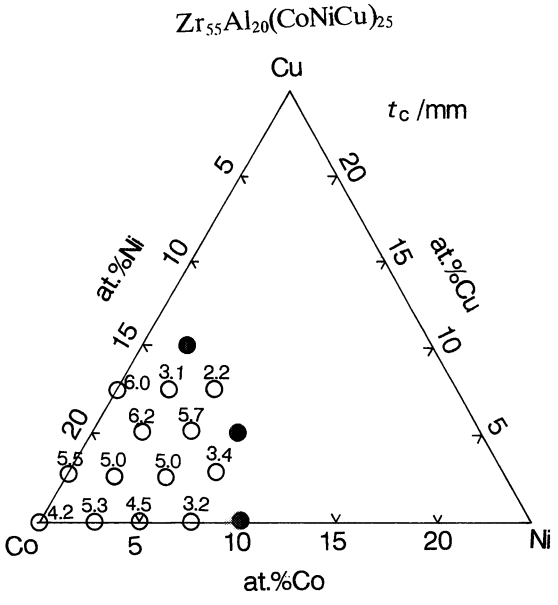

Fig. 3 Compositional dependence of the maximum sample thickness (t_c) for formation of an amorphous phase in $Zr_{55}Al_{20}(Co, Ni, Cu)_{25}$ alloys prepared by arc melting.

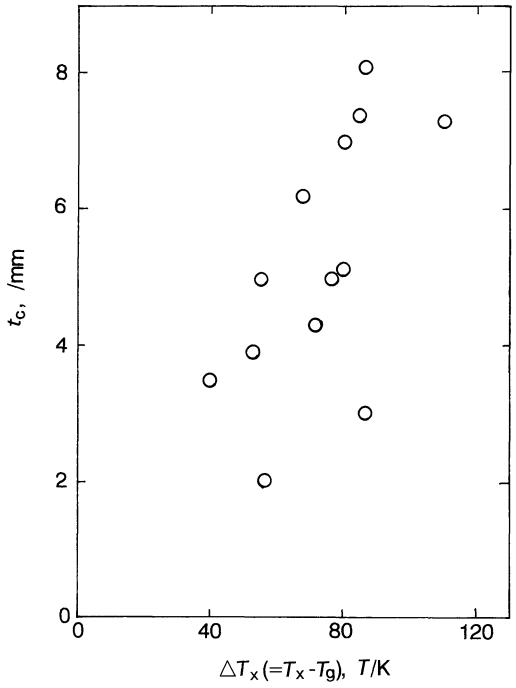

Fig. 4 Relation between t_c and the temperature interval of the supercooled liquid region, $\Delta T_x (=T_x - T_g)$ for amorphous $Zr_{60}Al_{10}(Co, Ni, Cu)_{30}$, $Zr_{60}Al_{15}(Co, Ni, Cu)_{25}$ and $Zr_{55}Al_{20}(Co, Ni, Cu)_{25}$ alloys.

ability is larger for the $Zr_{60}Al_{15}M_{25}$ system than for the other two alloy systems. In the comparison among these figures, one can notice an interesting tendency that the composition range in which the large glass-forming ability is obtained changes from the Cu-rich side to the Co-rich side through the Ni-rich side with increasing Al content. The change is consistent with the previous result that the largest glass-forming ability for each Zr-Al-M ternary system is obtained for Cu-rich $Zr_{65}Al_{7.5}Cu_{27.5}$[6], Ni-rich $Zr_{60}Al_{15}Ni_{25}$[5] and Co-rich $Zr_{55}Al_{20}Co_{25}$[7] alloys. All the amorphous alloys in Figs. 1 to 3 prepared by arc melting exhibit the distinct glass transition combined with a wide supercooled liquid region before crystallization. Figure 4 shows the relation between the critical sample thickness for formation of the amorphous phase by arc melting (t_c) and the temperature interval of the supercooled liquid region defined by the difference between the glass transition temperature (T_g) and the onset temperature of crystallization (T_x), $\Delta T_x (=T_x - T_g)$ for the Zr-Al-Co-Ni-Cu alloys. The weight of each alloy ingot used in the test was fixed to be 10 g. Although rather significant scatterings are seen, one can notice a tendency for t_c to increase with increasing ΔT_x, in agreement with that for Pd-Cu-Si, Pd-Ni-P and Pt-Ni-P glassy alloys[18]. The rather significant scatterings are presumed to reflect the scattering of t_c resulting from the heterogeneous nucleation of a crystalline phase. In any event, it is to be noticed that the bulky Zr-Al-Co-Ni-Cu ingot with the large thickness of about 7 mm can be vitrified by arc melting on a copper hearth cooled with water.

2. Thermal and mechanical properties of Zr-Al-Co-Ni-Cu amorphous alloys prepared by metallic mold casting

The application of the metallic mold casting process to the Zr-Al-Co-Ni-Cu alloys is expected to enable the formation of amorphous alloys with larger thicknesses as compared with those obtained by arc melting, when the heterogeneous nucleation is suppressed. In the subsequent study, it was clarified that the maximum diameter for formation of the amorphous cylinder by the metallic mold casting method reached about 7 mm for the $Zr_{60}Al_{10}Co_3Ni_9Cu_{18}$, $Zr_{60}Al_{15}Co_5Ni_{15}Cu_5$ and $Zr_{55}Al_{20}Co_{17.5}Ni_{2.5}Cu_5$ alloys with the largest t_c values in each Zr-Al-TM system. As an example, the temperature dependence of the apparent specific heat $C_{p,q}$ for the cast $Zr_{60}Al_{10}Co_3Ni_9Cu_{18}$ cylinder with a diameter of 5 mm is shown in Fig. 5, where the data of the melt-spun ribbon are also shown for comparison. The $C_{p,s}$ curve represents the specific heat of the sample which was once heated to the supercooled liquid region at 700 K. The heat of structural relaxation (ΔHr) defined by $\Delta Hr \equiv \int \Delta C_p (=C_{p,s} - C_{p,q}) dT$ is 147 J/mol for the cylindrical sample and 683 J/mol for the melt-spun ribbon, indicating that the cylindrical sample has a much relaxed structure as compared with that for the melt-spun ribbon, because of a much lower cooling rate in the metallic mold casting process. The much smaller ΔHr values were obtained for all the cast samples. However, no appreciable difference in T_g, T_x and ΔT_x is seen between the cast cylinder and the melt-spun ribbon, as seen in Fig. 5.

The cylindrical amorphous alloys prepared by the metallic mold casting method are thought to be formed at different cooling rates in the inner and outer surface regions. The different cooling rates are expected to cause the difference in mechanical properties, though no ap-

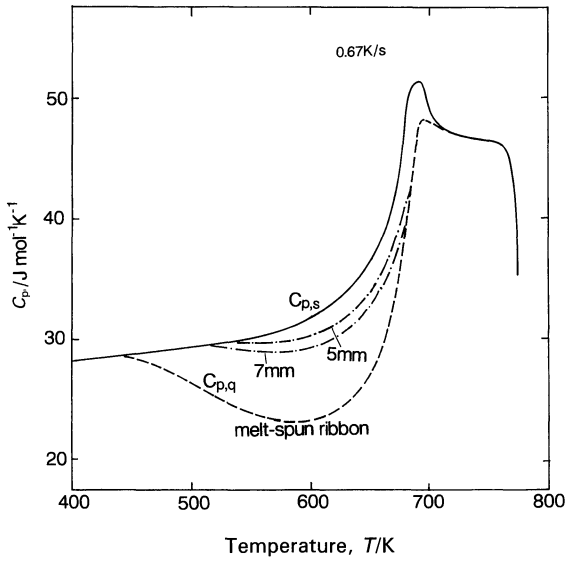

Fig. 5 The thermograms of amorphous $Zr_{60}Al_{10}Co_3Ni_9Cu_{18}$ cylinders with diameters of 5 and 7 mm. The data of the melt-spun ribbon are also shown for comparison.

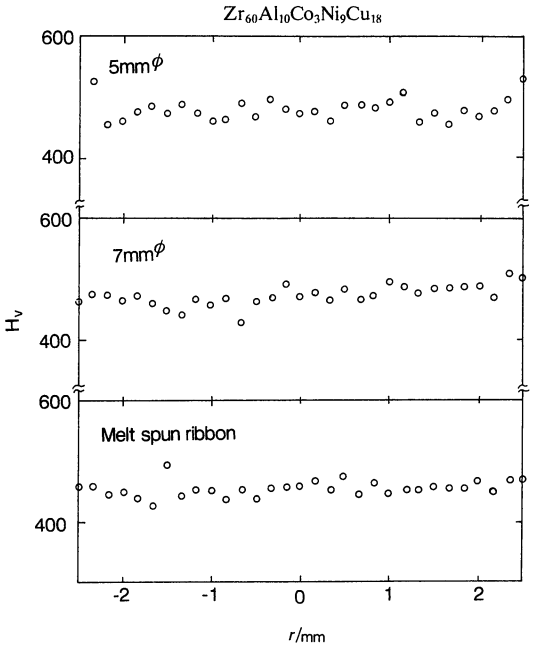

Fig. 6 Vickers hardness number as a function of the distance for the central point in the transverse cross section of amorphous $Zr_{60}Al_{10}Co_3Ni_9Cu_{18}$ cylinders with diameters of 5 and 7 mm prepared by copper mold casting. The data of the melt-spun amorphous ribbon with a thickness of 20 μm are also shown for comparison.

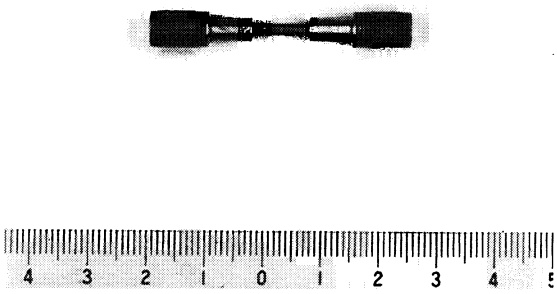

Fig. 7 Outer surface appearance of an amorphous $Zr_{60}Al_{10}Co_3Ni_9Cu_{18}$ alloy used for tensile testing.

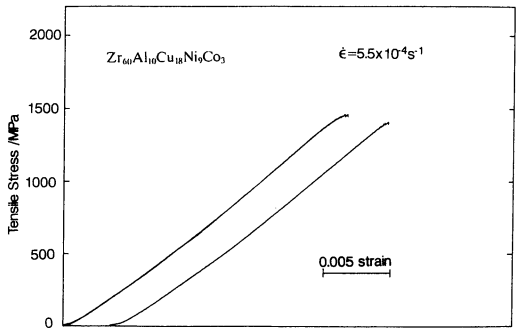

Fig. 8 Tensile stress-strain curves of amorphous $Zr_{60}Al_{10}Co_3Ni_9Cu_{18}$ cylinders.

preciable difference is detected for T_g, T_x and ΔT_x. Figure 6 shows the Vickers microhardness number as a function of the distance from the central point in the transverse cross-section for the cylindrical $Zr_{60}Al_{10}Co_3Ni_9Cu_{18}$ amorphous alloys with the diameters of 5 and 7 mm, along with the data as a function of the distance from the central point along the width direction for the corresponding melt-spun ribbon. The average H_v value is evaluated to be about 470 for the 5 mm cylinder and 475 for the 7 mm cylinder, in agreement with that (460) for the melt-spun ribbon. Furthermore, one cannot see any systematic change in H_v with the distance from the central point. These results indicate that the amorphous structure is independent of the distance from the central point, namely, the cooling rate. The formation of the nearly same amorphous structure is presumably because the cooling rate achieved by the metallic mold casting process is much larger than the critical cooling rate for formation of the amorphous phase.

It is expected that the amorphous Zr–Al–M alloys prepared at cooling rates higher than the critical cooling rate for glass formation exhibit high tensile strength comparable to that for the melt-spun amorphous ribbons, in spite of their bulky form with thicknesses above 5 mm. Figure 7 shows the outer surface appearance of the amorphous $Zr_{60}Al_{10}Co_3Ni_9Cu_{18}$ alloy which was used for the measurements of tensile strength and elongation. The test specimen was made by mechanical polishing from the as-cast amorphous cylinder with a diameter of 5 mm and a length of 50 mm. As seen in Fig. 7, the gauge dimension has a diameter of 2 mm and a length of 10 mm. The tensile stress-strain curves obtained for the two test specimens are shown in Fig. 8. It is seen that the alloy is subjected to elastic deformation, followed by yielding, slight plastic deformation accompanying a low degree of work hardening, distinct plastic flow accompanying serration and then final fracture. The feature of the stress-strain curve without significant work hardening and plastic elongation is in agreement with that for conventional amorphous metallic alloys with good bending ductility. However, it is particularly to be noticed that the distinct plastic flow accompanying serration takes place before final fracture. The observation of the serrated flow phenomenon during tensile deformation has hitherto been reported only for noble metal-based amorphous alloys of Pd- and Pt-based systems[18]. The generation of the serrated flow phenomenon implies that the shear deformation typical for ductile amorphous alloys does not occur catastrophically over the whole cross section and is once stopped at the deformation site. The momentary interupt of the shear deformation also implies the suppression of the final adiabatic fracture just after the shear deformation, indicating that the cast amorphous alloy has a highly ductile nature comparable to that for the noble-metal base amorphous alloys. The Young's modulus, yield stress defined by the deviation from the proportional relation, elastic elongation, plastic elongation and fracture stress are 97 GPa, 1390 MPa, 1.6%, 0.4% and 1510 MPa, respectively. It is shown in Fig. 6 that the Vickers hardness of the cast amorphous alloy is 475. Consequently, the values of $\varepsilon_{y,t}(=\sigma_y/E)$,

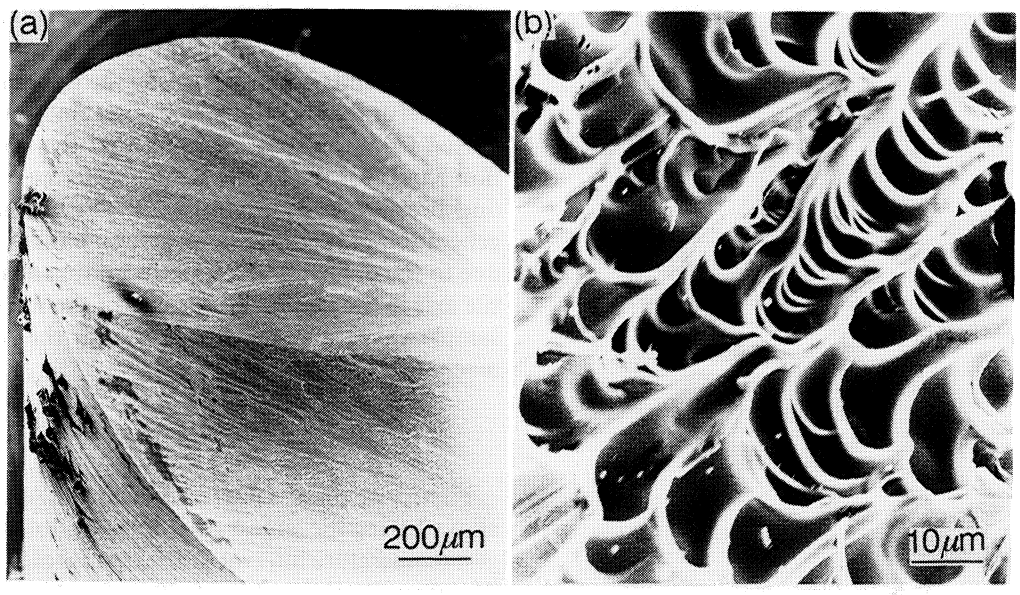

Fig. 9 Tensile fracture behavior (a) and fracture surface appearance (b) of an amorphous $Zr_{60}Al_{10}Co_3Ni_9Cu_{18}$ cylinder.

$\varepsilon_{y,c}(\fallingdotseq 3H_v/E)$ and σ_f/H_v are 0.14, 0.15 and 3.2, respectively. One can notice a rather good agreement between $\varepsilon_{y,t}$ and $\varepsilon_{y,c}$. Furthermore, the ratio of σ_f to H_v indicates that the amorphous solid deforms through an ideal elastic-plastic mode without work hardening. These results indicate that the present cast amorphous alloy has good ductility and exhibits the tensile deformation and fracture behavior which agrees with that for an ideal elastic-plastic material without work hardening.

Figure 9 shows the tensile fracture behavior and the tensile fracture surface appearance for the cast $Zr_{60}Al_{10}Co_3Ni_9Cu_{18}$ cylinder. The fracture occurs along the maximum shear plane which is declined by about 45 degrees to the tensile direction and the fracture surface consists of a well-developed vein pattern. As is evident from the comparison with the fracture surface appearance for the melt-spun amorphous ribbon sample with the same alloy composition shown in Fig. 10, the diameter of their veins is measured to be about 1 to 2 μm for the cast cylinder, being about 10 times as large as that (about 0.2 μm) for the melt-spun ribbon deformed at room temperature and comparable to that for the ribbon sample subjected to creep deformation at elevated temperatures near T_g. In addition, the SEM image shown in Fig. 11 reveals the remarkable development of the vein pattern caused by the adiabatic deformation at the final fracture stage. The remarkable development of the vein pattern and the significant increase in the diameter of the veins suggest that the temperature during the final adiabatic fracture increases because of the suppression of the final fracture resulting from the good ductility. Furthermore, the increase in the diameter of the veins also implies the increase in the thickness of the shear deformation region which causes the increase in the energy required for plastic deformation and final fracture.

The compressive test method is thought to be more appropriate for the more detailed investigation of the serrated flow phenomenon and the work-hardening behavior. Figure 12 shows the compressive stress-strain curves for the two cast $Zr_{60}Al_{10}Co_3Ni_9Cu_{18}$ cylindrical samples with a diameter of 2.5 mm and a height of 5.0 mm. In comparison with those (Fig. 8) obtained by tensile test, one can notice that the serration generates in a wider strain region from the yield point to the final fracture stage while no appreciable difference in the total strain up to final fracture is seen. Furthermore, the degree of the work hardening accompanying the serrated flow is slightly larger for the compressive test sample. The further development of the serrated flow and the slight increase in the degree of work hardening are presumably because the shear deformation bands generate along the whole outer

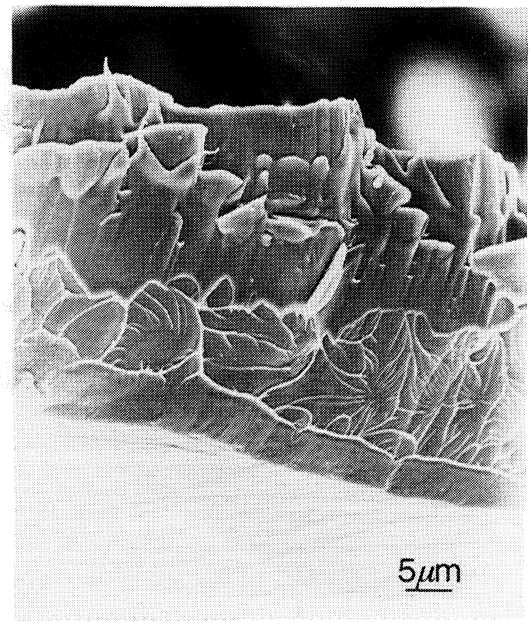

Fig. 10 Tensile fracture surface appearance of an amorphous $Zr_{60}Al_{10}Co_3Ni_9Cu_{18}$ ribbon prepared by melt spinning.

Fig. 11 Tensile fracture surface appearance of an amorphous $Zr_{60}Al_{10}Co_3Ni_9Cu_{18}$ cylinder.

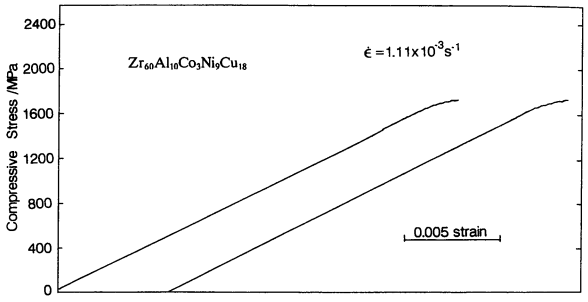

Fig. 12 Compressive stress-strain curves of amorphous $Zr_{60}Al_{10}Co_3Ni_9Cu_{18}$ cylinders.

surface for the compressive sample as shown in Fig. 13 and the massive movement of the constituent atoms in the shear bands is suppressed by the crossing among the shear deformation bands. This presumption is also supported from the contrast result that the shear deformation bands for the tensile sample generate only along the one direction as shown in Fig. 9. The inclination for the generation of the shear deformation bands is presumably due to the difficulty of the perfect adjustment of the tensile axis in the tensile test because of the scatterings in the sample shape and the tensile axis in the tensile testing machine.

IV. Discussion

Firstly, we discuss the reason why the Al content in the alloys having the largest glass-forming ability and the largest temperature interval of the supercooled liquid region decreases in the order of 20% for M=Co, 15% for M=Ni and then 7.5% for M=Cu. It has previously been reported[7][19] that the large glass-forming ability and the wide supercooled liquid region are achieved by the increase in the liquid/solid interfacial energy through the formation of a highly dense random packed structure. Furthermore, the increase in the degree of the dense random packing is thought to be attributed to appropriate atomic size ratios among the constituent elements. Based on the above-described concept on the stability of the supercooled liquid, the decrease in Al content for the achievement of the largest glass-forming ability in the Zr–Al–Cu system may be due to the larger atomic size for Cu than for Co and Ni. The smaller atomic size ratio between Al and Cu seems to cause the decrease in an optimum Al content for the achievement of the highest stability of the supercooled liquid. Furthermore, it is thought that the alloy composition of the alloys with the largest glass-forming ability lies in the pseudo binary Zr_2Al–

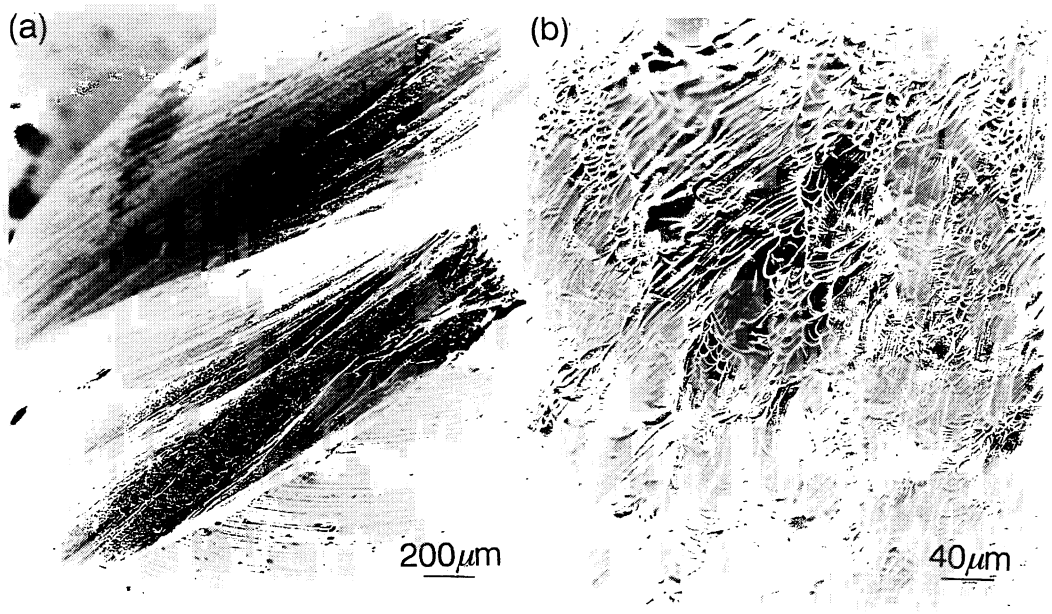

Fig. 13 Compressive fracture behavior of an amorphous $Zr_{60}Al_{10}Co_3Ni_9Cu_{18}$ cylinder.

Zr_2M system. From the fact[20] that the melting (or decomposition) temperature is about 1523 K for Zr_2Al, 1373 K for Zr_2Co, 1423 K for Zr_2Ni and 1293 K for Zr_2Cu, the addition of Al into Zr_2Cu causes a significant increase in melting temperature in a high Al concentration range. On the contrary, the replacement of Co or Ni in Zr_2M by Al does not cause any significant increase in melting temperature even in a high Al concentration range. The nearly constant melting temperature is favorable for the dissolution of a larger amount of Al into the Zr_2M alloys, resulting in the maintenance of the large glass-forming ability. Besides, the decrease in the optimum Al content in the Zr-Al-Cu system seems to be related to the significant changes in the type and size of the unit cell between Zr_2Cu and Zr_2Co or Zr_2Ni[21]. That is, the Zr_2Cu compound has a bct structure with lattice parameters of $a=0.32204$ nm and $c=1.11832$ nm while the Zr_2Co and Zr_2Ni compounds have a tetragonal structure with lattice parameters of $a=0.6336$ nm and $c=0.54690$ nm and $a=0.6477$ nm and $c=0.5241$ nm, respectively. Considering that the Zr_2Al compound has a tetragonal structure with $a=0.4894$ nm and $c=0.5928$ nm, the difference in the unit size is concluded to be less than 11% between Zr_2Al and Zr_2Co or Zr_2Ni compounds. The similarity of the lattice parameters may also be one of the factors which lead to the increase in the optimum Al content for the achievement of the largest glass-forming ability, as compared with the lower Al concentration for the Zr-Al-Cu system where the lattice parameters between Zr_2Al and Zr_2Cu are significantly different. Although the most dominant factor for the difference in the optimum Al content remains unclear in the present study, the difference is presumed to result from the combination of the above-described three factors.

Secondly, we investigate the dominant factor for the achievement of the large glass-forming ability for the Zr-Al-Co-Ni-Cu quaternary and penternary alloys. The reduced glass transition temperature (T_g/T_m) measured in the present study is in the rather narrow range of 0.59 to 0.67 and no distinct correspondence is seen between T_g/T_m and the glass-forming ability evaluated by the critical sample thickness (t_c) for the formation of an amorphous single phase for the arc-melted ingots. On the other hand, the t_c values have a close relation to the temperature interval of supercooled liquid region, $\Delta T_x(=T_x-T_g)$, as shown in Fig. 4, though significant scatterings reflecting the ease of the heterogeneous nucleation of a crystalline phase are seen. The close relation indicates that the large glass-forming ability is dominated by the stability of the supercooled liquid against crystallization. In the framework of homogeneous nucleation and growth theory from liquid, the dominant factors in a constant supercooled state have been pointed out[22] to be viscosity, liquid/solid interfacial energy and the size of a crystalline nucleus. The theory indicates that there is a clear tendency for the glass-forming ability to increase with an increase in the temperature dependence of viscosity, the liquid/solid interface energy and the size of a crystalline nuclei. Among the three factors, the temperature dependence of viscosity, $\eta(T)$, corresponds to T_g/T_m and the larger the $\eta(T)$ the higher is the T_g/T_m. It is described that no linear relation is seen between T_g/T_m and t_c for the present Zr-Al-Co-Ni-Cu alloys. Consequently, it is thought that the viscosity is not the most dominant factor for the large glass-forming ability of the present alloys. The good liner relation between t_c and ΔT_x indicates that the liquid/solid interface energy is more dominant because ΔT_x is dominated by the energy. It has been previously described[7][19] that the large liquid/solid interface energy for the present alloys is due to the formation of a highly dense random packed structure resulting from the constituent elements with significantly different atomic sizes and large negative heats of mixing. Furthermore, the striking effect of the multicomponents on the increase in the glass-forming ability is also attributed to the increase in the critical size of a crystalline nuclei resulting from the formation of multicomponent clusters in the supercooled liquid, in addition to the increase in the liquid/solid interface energy.

Finally, it is also important to investigate the reason for the extremely large glass-forming ability by taking account of the experimental data on the peak temperatures for nucleation and growth rates in the supercooled liquid. It has been previously pointed out[23] that in the relation between $(1/T_p-1/T_{po})$ and pre-annealing temperature (T_a), the peak temperature corresponds to the temperature at which the nucleation rate of a crystalline phase is maximum. Here, T_{po} and T_p represent the temperatures at which the exothermic peak on the DSC curve takes place for the as-quenched sample and the pre-annealed sample, respectively. Furthermore, the temperature where the exothermic peak on the DSC curve measured at a heating rate as fast as possible appears can be regarded as the maximum temperature for the growth of a crystalline phase. As plotted for $Zr_{70}Cu_{30}$, $Zr_{65}Al_{7.5}Cu_{27.5}$ and $Zr_{65}Al_{7.5}Ni_{10}Cu_{17.5}$ alloys in Fig. 14, a distinct maximum phenomenon is observed for the Zr-Al-Cu and Zr-Al-Co-Ni-Cu alloys at 688 and 679 K, respectively, which are lower by 143 K and 152 K, respectively, than the crystallization temperature measured at a high heating rate of 5.3 K/s. On the other hand, no isolated peak is seen for the Zr-Cu binary alloy. This result indicates that the maximum nucleation temperature of crystalline phase is significantly different from the maximum growth temperature for the Zr-Al-Cu and Zr-Al-Co-Ni-Cu alloys with wide supercooled liquid regions before crystallization while their maximum temperatures lie in the nearly same temperature range for the Zr-Cu alloy with the narrow supercooled liquid region. The significant difference in the peak temperature between nucleation and growth reactions also plays an important role in the appearance of the wide supercooled liquid region before crystallization. The distinct splitting phenomenon for the nucleation and growth peaks also comes from the retardation of the growth reaction of a crystalline phase in the present highly dense random packed structure. The retardation is due to the difficulty in the atomic rearrangement on a long-range scale in the highly dense random

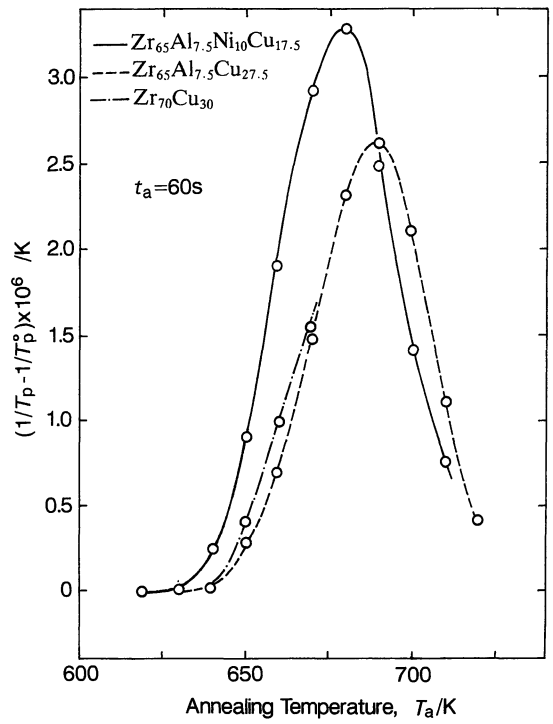

Fig. 14 Relation between $(1/T_p - 1/T_{po})$ and pre-annealing temperature (T_a) for amorphous $Zr_{70}Cu_{30}$, $Zr_{65}Al_{7.5}Cu_{27.5}$ and $Zr_{65}Al_{7.5}Ni_{10}Cu_{17.5}$ alloys. T_p and T_{po} represent the temperatures at which the exothermic peak on the DSC curve appears for the as-quenched and pre-annealed states, respectively. The pre-annealing time at T_a was fixed to be 60 s.

packed structure.

In any event, the above-described results and discussion allow us to derive the following concept that a further multiplication of alloy components with appropriate atomic sizes and attractive bonding states enables the preparation of a new amorphous alloy with larger glass-forming ability.

V. Summary

In order to search an appropriate alloy composition for the preparation of bulky amorphous alloys exhibiting high tensile strength and good ductility, we examined the compositional dependence of the critical sample thickness for formation of an amorphous phase in the alloy ingots of the $Zr_{60}Al_{10}M_{30}$, $Zr_{60}Al_{15}M_{25}$ and $Zr_{55}Al_{20}M_{25}$ (M=Co, Ni, Cu) systems prepared by arc melting. The largest thickness is 6.1 mm for $Zr_{60}Al_{10}Co_3Ni_9Cu_{18}$, 6.8 mm for $Zr_{60}Al_{15}Co_5Ni_{15}Cu_5$ and 6.2 mm for $Zr_{55}Al_{20}Co_{17.5}Ni_{2.5}Cu_5$. The appropriate alloy composition changes in the order of Cu-rich, Ni-rich and Co-rich with increasing Al content from 10 to 20%. The application of the metallic mold casting method to the three alloys enabled the formation of amorphous cylinders with the largest diameter of about 7 mm. The large glass-forming ability is due to the increase in the liquid/solid interface energy and in the size of a crystalline nuclei through the formation of a highly dense random packed structure resulting from the multiplication of alloy components with significantly different atomic sizes. No appreciable difference in T_g and T_x is seen between the cast alloy with a diameter of 5 mm and the melt-spun ribbon with a thickness of 20 μm, though the heat of structural relaxation is smaller by about 78% for the cast alloy. The cylindrical 10%Al alloy subjected to tensile test was deformed plastically, accompanying the generation of distinct serrated flow, and the degree of the serrated flow increases by the change to the compressive testing mode. The generation of the serrated flow phenomenon is due to the momentary interupt of the shear sliding resulting from the highly ductile nature of the glassy alloy. The Young's modulus, tensile yield strength, fracture strength and elongation for the 10%Al alloy are 97 GPa, 1390 MPa, 1510 MPa and 2.0%, respectively. The fracture surface consists mainly of a remarkably developed vein pattern which reflects the highly ductile nature. The success of the preparation of the cast amorphous Zr–Al–M alloys exhibiting high tensile strength and good ductility is important for the subsequent progress of metallic glassy materials.

REFERENCES

(1) A. Inoue, K. Ohtera, K. Kita and T. Masumoto: Jpn. J. Appl. Phys., **27** (1988), L2248.
(2) A. Inoue, M. Kohinata, K. Ohtera, A. P. Tsai and T. Masumoto: Mater. Trans., JIM, **30** (1989), 378.
(3) A. Inoue, T. Zhang and T. Masumoto: Mater. Trans., JIM, **30** (1989), 965.
(4) A. Inoue, H. Yamaguchi, T. Zhang and T. Masumoto: Mater. Trans., JIM, **31** (1990), 104.
(5) A. Inoue, T. Zhang and T. Masumoto: Mater. Trans., JIM, **31** (1990), 177.
(6) T. Zhang, A. Inoue and T. Masumoto: Mater. Trans., JIM, **32** (1992), 1005.
(7) A. Inoue, T. Zhang and T. Masumoto: J. Non-Cryst. Solids, **156–158** (1993), 473.
(8) A. Inoue, N. Nishiyama, K. Amiya, T. Zhang and T. Masumoto: Mater. Lett., **19** (1994), 131.
(9) A. Inoue, K. Amiya, I. Yoshii, N. Nishiyama and T. Masumoto: Mater. Sci. Eng., **A179/A180** (1994), 692.
(10) A. Inoue, T. Zhang and T. Masumoto: Mater. Trans., JIM, **31** (1990), 425.
(11) A. Inoue, A. Kato, T. Zhang, S. G. Kim and T. Masumoto: Mater. Trans., JIM, **32** (1991), 609.
(12) A. Inoue, T. Nakamura, N. Nishiyama and T. Masumoto: Mater. Trans., JIM, **33** (1992), 937.
(13) A. Inoue, T. Nakamura, T. Sugita, T. Zhang and T. Masumoto: Mater. Trans., JIM, **34** (1993), 351.
(14) A. Inoue, K. Onoue, Y. Horio and T. Masumoto: Sci. Rep. Res. Inst. Tohoku Univ., **A39** (1994), 147.
(15) A. Inoue, K. Kita, T. Zhang and T. Masumoto: Met. Trans., JIM, **30** (1989), 722.
(16) A. Inoue, T. Zhang, N. Nishiyama, K. Ohba and T. Masumoto: Mater. Trans., JIM, **33** (1993), 1234.
(17) A. Inoue, T. Zhang, N. Nishiyama, K. Ohba and T. Masumoto: Mater. Sci. Eng., **A179/A180** (1994), 210.
(18) H. S. Chen: Rep. Prog. Phys., **43** (1980), 353.
(19) A. Inoue: Proc. of ISMANAM, Grenoble, June 1994, in press.
(20) *Binary Phase Diagrams*, ed. by T. B. Massalski, ASM Intern., Materials Park, Ohio, (1990).
(21) W. B. Pearson: *Lattice Spacings and Structures of Metals and Alloys*, Pergamon Press, London, (1958).
(22) D. R. Uhlmann and H. Yinnon: *Glass Science and Technology*, Vol. 1, ed. by D. R. Uhlmann and N. J. Kreidl, Academic Press, New York, (1983) p. 1.
(23) X. Zhou and M. Yamane: J. Ceramic Association Japan, **96** (1988), 152.